Conservative Locally Moving Mesh Method for Multifluid Flows

Alina Chertock[†]

[†]*Department of Mathematics, North Carolina State University, Raleigh, NC 27695*

chertock@math.ncsu.edu

Alexander Kurganov[⋆]

[⋆]*Mathematics Department, Tulane University, New Orleans, LA 70118*

kurganov@math.tulane.edu

Abstract

We present a conservative locally moving mesh finite-volume-particle method for computing compressible multifluids flows. The idea behind the new method is to use different schemes for the flow and the interface tracking: the Euler equations are numerically integrated using a finite-volume scheme, while a particle method is used to track the moving interface and obtain a subcell information needed to create an adaptive locally moving mesh such that the material interface always coincides with the moving cell boundary. The method does not generate significant oscillations across the material interface and provides an enhanced resolution of the contact discontinuities.

Key words : multicomponent fluids, conservation laws, finite-volume schemes, particle methods, central-upwind schemes, locally moving mesh.

1 Introduction

The research of numerical methods for conservation laws has been motivated to a large extent by its application to gas dynamics, where the governing equations can be written as a system of conservation laws. For example, in the one-dimensional (1-D) case, the Euler equations of gas dynamics express conservation of mass, momentum and energy:

$$\begin{pmatrix} \rho \\ \rho u \\ E \end{pmatrix}_t + \begin{pmatrix} \rho u \\ \rho u^2 + p \\ u(E+p) \end{pmatrix}_x = 0, \tag{1}$$

Here, ρ is the density, u is the velocity, E is the total energy, and p is the pressure. The system is completed by adding the equation of state (EOS), which in the case of ideal gases, reads

$$p = (\gamma - 1)\left(E - \frac{1}{2}\rho u^2\right), \quad \gamma = \text{const.} \tag{2}$$

Multicomponent compressible flows occur in many situations, in which fluids have different physical properties and are separated by interfaces. This paper is concerned, but not limited, to fluids that consist of two ideal gases with different values of γ, which is assumed to be a piecewise constant function propagating with the fluid velocity u according to the following equation:

$$\gamma_t + u\gamma_x = 0, \tag{3}$$

which can be also written in the conservative form:

$$(\rho\gamma)_t + (u\rho\gamma)_x = 0. \tag{4}$$

We note that in addition to the γ-model (1)–(3), introduced in [ROE 84], several alternative models (such as the mass fraction and the level-set models) for multicomponent computations have been suggested and extensively studied. For description of some of them we refer the reader to [ABG 01b] and the references therein.

Most commonly used numerical methods for the Euler equations of gas dynamics are shock-capturing finite-volume (FV) methods (see, e.g., [KRÖ 97, LEV 02]). One of the simplest, most efficient and robust FV methods are the Godunov-type central-upwind schemes originally introduced in [KUR 00b, KUR 01] and then further improved in [KUR]. These schemes enjoy all the major advantages of Riemann-problem-solver-free central schemes, and at the same time, have a certain "built-in" upwind nature. However, it is well-known that the numerical dissipation, present in these, as well as in any other FV methods, typically prevents sharp resolution of contact waves. In the case of compressible multifluid Euler equations, capturing contact discontinuities accurately is even more difficult since conservative algorithms (based on the conservation of total mass, momentum, and energy) may lead to non-physical oscillations near material interfaces and to radical changes in the equation of state across the interface (see, e.g., [ABG 01b]).

In the past decade, several methods that are capable to overcome this difficulty have been proposed. Most of them (including the consistent primitive algorithm [KAR 94], a combination of shock-capturing and front-tracking methods [COC 97], the ghost fluid method [FED 99], and the ghost fluid method for the poor [ABG 01a, ABG 01b]) are designed to prevent pressure oscillations and to enhance a resolution of contact discontinuities. However, these methods do not conserve the total energy, which may lead to capturing wrong weak solutions, especially in the multidimensional case, when long time interactions between shock and contact waves are possible. Therefore, the development of non-oscillatory conservative multifluid algorithms is an important and challenging task.

A new approach that allows the conservation of the total energy without producing pressure oscillations has been recently introduced in [WAC 04] through a model,

in which an equation for the energy of one of the fluids has been added to the system (1)–(3). However, the added equation contains nonconservative products and thus validity of the model in the presence of shock waves is questionable.

The aim of the current work is to introduce a new numerical method for the original system (1)–(2),(4) that achieves the same goals: the conservation of total energy and lack of oscillations across the material interface. The new method is based on the ideas introduced in [CHE 04, CHEa, CHEb]: a FV scheme is applied to the system (1)–(2), while the transport equation (4) is solved by a particle method. By doing so we take an advantage of the nondissipativeness of the particle method, and thus a very high resolution in capturing material interfaces is guaranteed. We use the particle method to track the moving interface and obtain a subcell information needed to create an adaptive locally moving mesh such that the material interface always coincides with the moving cell boundary. The proposed *locally moving mesh finite-volume-particle method* consists of two main steps. First, the solution is evolved to a new time level using a conservative FV scheme (the central-upwind scheme or any other scheme with a numerical flux that satisfies essentially three-point consistency). This leads to pressure oscillations, which are then eliminated in the correction step — the evolved solution is projected onto the new locally adapted grid. A special conservative projection procedure is described in §2.1, where we also prove that if a FV scheme satisfies essentially three-point consistency, then for a single contact wave a perfect resolution is achieved. Obviously, in the examples with (initial) wave interactions, one cannot get a perfect resolution, but no significant pressure oscillations have been observed in the performed numerical experiments, and the quality of the computed solution is comparable with the one obtained in the single fluid case.

2 Finite-Volume-Particle Method

We begin with a brief description of the *semi-discrete central-upwind* schemes used to numerically solve the system (1)–(2). For a complete description and derivation of these schemes, we refer the reader to [KUR 01, KUR].

Let us introduce a spatial grid, in which the cells $(x_{j-\frac{1}{2}}, x_{j+\frac{1}{2}})$ of size $\Delta x_j := x_{j+\frac{1}{2}} - x_{j-\frac{1}{2}}$ are centered at the points $x = x_j$; denote the vector of conservative variables by $\mathbf{w} := (\rho, \rho u, E)^T$; and assume that at some time level t, the (computed) solution, realized in terms of its cell averages, $\bar{\mathbf{w}}_j(t) := \frac{1}{\Delta x_j}\int_{x_{j+1/2}}^{x_{j-1/2}} \mathbf{w}(x,t)\,dx$, is available. We use $\bar{\mathbf{w}}_j(t)$ to reconstruct a global, (essentially) non-oscillatory, conservative piecewise polynomial interpolant:

$$\widetilde{\mathbf{w}}(x;t) = \mathcal{P}_j(x;t), \qquad x_{j-\frac{1}{2}} < x < x_{j+\frac{1}{2}}, \quad \forall j. \tag{5}$$

The cell averages are evolved in time according to the semi-discrete central-upwind scheme:

$$\frac{d}{dt}\bar{\mathbf{w}}_j(t) = -\frac{\mathbf{H}_{j+\frac{1}{2}}(t) - \mathbf{H}_{j-\frac{1}{2}}(t)}{\Delta x_j}, \tag{6}$$

where the numerical fluxes $\mathbf{H}_{j+\frac{1}{2}}$ are given by

$$\mathbf{H}_{j+\frac{1}{2}}(t) := \frac{a^+_{j+\frac{1}{2}}\mathbf{f}(\mathbf{w}^-_{j+\frac{1}{2}}) - a^-_{j+\frac{1}{2}}\mathbf{f}(\mathbf{w}^+_{j+\frac{1}{2}})}{a^+_{j+\frac{1}{2}} - a^-_{j+\frac{1}{2}}} + a^+_{j+\frac{1}{2}}a^-_{j+\frac{1}{2}}\left[\frac{\mathbf{w}^+_{j+\frac{1}{2}} - \mathbf{w}^-_{j+\frac{1}{2}}}{a^+_{j+\frac{1}{2}} - a^-_{j+\frac{1}{2}}} - \mathbf{q}_{j+\frac{1}{2}}\right]. \quad (7)$$

Here, $\mathbf{f}(\mathbf{w}) := (\rho u, \rho u^2{+}p, u(E{+}p))^T$ is the flux vector function, $\mathbf{w}^-_{j+\frac{1}{2}} := \mathcal{P}_j(x_{j+\frac{1}{2}}; t)$ and $\mathbf{w}^+_{j+\frac{1}{2}} := \mathcal{P}_{j+1}(x_{j+\frac{1}{2}}; t)$ are the corresponding left and right values of the reconstruction (5) at the cell interface $x = x_{j+\frac{1}{2}}$, where $\widetilde{\mathbf{w}}(\cdot; t)$ is generically discontinuous. At time $t+$, the discontinuity splits, in general, into three waves, whose largest *left-* and *right-sided speeds*, $a^-_{j+\frac{1}{2}}$ and $a^+_{j+\frac{1}{2}}$, can be estimated by

$$a^-_{j+\frac{1}{2}} = \min\left\{(u{-}c)^-_{j+\frac{1}{2}}, (u{-}c)^+_{j+\frac{1}{2}}, 0\right\}, \quad a^+_{j+\frac{1}{2}} = \max\left\{(u{+}c)^-_{j+\frac{1}{2}}, (u{+}c)^+_{j+\frac{1}{2}}, 0\right\}, \quad (8)$$

where $c = \sqrt{\gamma p/\rho}$ is a speed of sound. Finally, $\mathbf{q}_{j+\frac{1}{2}}$ is an "anti-diffusion" term that reduces the numerical dissipation. It has been rigorously derived via the projection-evolution approach in [KUR], see also [KUR 00a, CHE 04].

Note that all the quantities on the right-hand side (RHS) of (7) are functions of t but we drop this dependence in order to simplify the notation.

Remark 1 The non-oscillatory behavior of the central-upwind schemes hinges on an appropriate choice of a piecewise polynomial reconstruction and the formal spatial order of accuracy of the scheme is determined by the order of the reconstruction. For example, the second-order central-upwind scheme should employ a non-oscillatory piecewise linear reconstruction — a variety of such reconstructions is available (see, e.g., [SWE 84, KRÖ 97, LEV 02, LIE 03]). The formal temporal order of accuracy is determined by the order of the ODE solver used to integrate the system (6).

Next, we briefly describe the second main ingredient of our new method — the particle method — used to solve the transport equation (4). We seek a solution of (4) as a linear combination of Dirac distributions, $(\rho\gamma)_N(x,t) = \sum_{i=1}^{N} \alpha_i \delta(x - \hat{x}_i(t))$, whose positions, $\hat{x}_i$, and coefficients, α_i, represent locations and weights of the particles, respectively, and N is a total number of particles. Considering a weak formulation of the problem and substituting $(\rho\gamma)_N(x,t)$ into (4) results in the following system of ODEs for the locations of the particles:

$$\frac{d\hat{x}_i(t)}{dt} = u(\hat{x}_i, t). \quad (9)$$

The initial positions of the particles, $\hat{x}_i(0)$, and their weights, α_i, are to be chosen to provide a high-order approximation to the initial data, $(\rho u)(x, 0)$. For example, one can initially place the particles into the centers of the FV cells and take the weights to be $\alpha_i = \int_{x_{i-1/2}}^{x_{i+1/2}} (\rho u)(x,0)\, dx$. Note that since equation (4) is homogeneous, the weights α_i do not change in time, which would not be true in the presence of, say, a chemical reaction term on the RHS of (4), see, e.g., [CHEa].

Since the conservative gas dynamics variables can be evolved to the next time level according to the system (1)–(2) independently of the transport equation (4), the velocities $u(\hat{x}_i(t),t)$ on the RHS of (9) can be calculated from the piecewise polynomial reconstructions of ρu and ρ, used for solving (1)–(2) by the central-upwind scheme. Notice that since u may be discontinuous, the RHS of (9) may be discontinuous as well. However, as long as the RHS of (9) is bounded, the existence of its generalized solution is guaranteed by the theory of Filippov [FIL 64, FIL 88]. In practice, u is a piecewise smooth function with a finite number of discontinuities only, and therefore one can numerically solve (9) by the same ODE solver used to solve the system (6).

In order to obtain the values of γ needed in the EOS (2), the point values of $\rho\gamma$ should, in principle, be recovered from its particle distribution at every time step. However, it is known (see, e.g., [CHE 04, CHEa]) that for discontinuous solutions a standard recovery procedure, based on the regularization of a particle solution by taking a convolution with a so-called cutoff function [RAV 85], may lead to either smearing or oscillations near the material interface. This would produce unphysical values of γ, which are unacceptable in the problem under consideration. Therefore, we use the method, proposed in [CHE 04], that allows to completely avoid any loss of resolution attributed to the regularization of the particle distribution. The idea is to consider equation (3) for γ, which is dual to equation (4), and hence the point values of its solution are:

$$\gamma(\hat{x}_i(t),t) = \gamma(\hat{x}_i(0),0),$$

where $\hat{x}_i(t)$ are solutions of the system (9). Note that in this case, the particle method for $\rho\gamma$ reduces to the method of characteristics for γ. However, one can verify that this will no longer be true if the RHS of (4) is nonzero, as illustrated in [CHE 04].

Remark 2 We use two different grids in our hybrid method: a grid for the central-upwind scheme, $\{x_j\}$, which may be initially uniform but then is locally adjusted so that the material interface coincides with a cell interface at every time step (see §2.1); and particle locations, $\{\hat{x}_i(t)\}$, that change in time according to the flow.

2.1 Locally Moving Mesh Algorithm

We assume that at some time level t a solution of (1)–(4), realized by the cell averages of the conserved quantities, $\{\bar{\mathbf{w}}(t)\}$, and by the particle locations, $\{\hat{x}_i(t)\}$, has been computed. We also assume that the fluids are separated, that is, at the first I particles the value of γ is γ_l, while $\gamma(x_{I+1}) = \ldots = \gamma(x_N) = \gamma_r$, and that the material interface, defined by $\hat{x}_{\text{int}} := (\hat{x}_I + \hat{x}_{I+1})/2$, coincides with the boundary between the J-th and the $(J+1)$-st cells, $x_{J+\frac{1}{2}}$. The proposed evolution algorithm consists of the following 6 steps.

1. Evolve the conserved quantities from time t to time $t+\Delta t$ in each cell by applying the central-upwind scheme (6)–(7) to the system (1) with the EOS (2) with $\gamma = \gamma_l$ for $x < x_{J+\frac{1}{2}}$ and $\gamma = \gamma_r$ for $x > x_{J+\frac{1}{2}}$.

At this point, the evolved solution is averaged across the material interface, which has moved and is no longer located exactly at $x = x_{J+\frac{1}{2}}$. This would lead to pressure

oscillations, and thus we have to correct the evolved solution near the interface. In the following, we assume that the velocity u is positive at the interface, which is thus moving to the right. The case of negative u can be treated similarly.

2. Compute the cell averages of $\mathbf{w}(t+\Delta t)$ over the "double-cell" $(x_{J-\frac{1}{2}}, x_{J+\frac{3}{2}})$:

$$\bar{\mathbf{w}}_{\mathrm{J,J+1}} := \frac{\Delta x_J \bar{\mathbf{w}}_J + \Delta x_{J+1}\bar{\mathbf{w}}_{J+1}}{\Delta x_J + \Delta x_{J+1}}. \tag{10}$$

These cell averages are to be redistributed over the new locally adapted cells.

3. By solving (9), evolve particles to the new locations, $\{\hat{x}_i^{\mathrm{new}} := \hat{x}_i(t+\Delta t)\}$, and compute the new fluid interface: $\hat{x}_{\mathrm{int}}^{\mathrm{new}} := (\hat{x}_I^{\mathrm{new}} + \hat{x}_{I+1}^{\mathrm{new}})/2$. Note that the CFL condition ensures that the interface is now located in the cell $(x_{J+\frac{1}{2}}, x_{J+\frac{3}{2}})$.

4. Adjust the grid by moving the point $x_{J+\frac{1}{2}}$ to its new location $x_{J+\frac{1}{2}}^{\mathrm{new}} := \hat{x}_{\mathrm{int}}^{\mathrm{new}}$, so that the new cells near the interface will be $(x_{J-\frac{1}{2}}, x_{J+\frac{1}{2}}^{\mathrm{new}})$ and $(x_{J+\frac{1}{2}}^{\mathrm{new}}, x_{J+\frac{3}{2}})$.

5. This is the key step, in which the computed solution is projected onto the new, locally adjusted mesh. This should be done in such a way that the conservation is preserved and pressure oscillations are eliminated. In particular, the latter means that in the case of a single contact wave, both u and p should remain constant across the interface (see Proposition 2.1 below).

These goals are achieved by computing the projected cell averages over the new J-th and $(J+1)$-st cells, $\bar{\mathbf{w}}_J^{\mathrm{new}}$ and $\bar{\mathbf{w}}_{J+1}^{\mathrm{new}}$, in the following manner. Let $\bar{w}$ be one of the components of the vector $\bar{\mathbf{w}}$, and $\bar{w}_{J,J+1}$ its corresponding "double-cell" average (10). If $\bar{w}_{J,J+1}$ is a local extremum, then no conservative correction is possible and we thus take:

$$\bar{w}_J^{\mathrm{new}} = \bar{w}_{J,J+1}, \qquad \bar{w}_{J+1}^{\mathrm{new}} = \bar{w}_{J,J+1}.$$

If the solution is locally monotone, that is, if $(\bar{w}_{J-1} - \bar{w}_{J,J+1})(\bar{w}_{J,J+1} - \bar{w}_{J+2}) > 0$, then the new cell averages are:

$$\bar{w}_J^{\mathrm{new}} = \frac{\Delta x_J^{\mathrm{new}} \bar{w}_{J,J+1} + \delta}{\Delta x_J^{\mathrm{new}}}, \qquad \bar{w}_{J+1}^{\mathrm{new}} = \frac{\Delta x_{J+1}^{\mathrm{new}} \bar{w}_{J,J+1} - \delta}{\Delta x_{J+1}^{\mathrm{new}}}, \tag{11}$$

where

$$\Delta x_J^{\mathrm{new}} = x_{J+\frac{1}{2}}^{\mathrm{new}} - x_{J-\frac{1}{2}}, \qquad \Delta x_{J+1}^{\mathrm{new}} = x_{J+\frac{3}{2}} - x_{J+\frac{1}{2}}^{\mathrm{new}},$$

and

$$\delta = \mathrm{sgn}(\bar{w}_{J,J+1} - \bar{w}_{J-1})\ \min\Big\{|\bar{w}_{J,J+1} - \bar{w}_{J-1}|\Delta x_J^{\mathrm{new}},\ |\bar{w}_{J+2} - \bar{w}_{J,J+1}|\Delta x_{J+1}^{\mathrm{new}}\Big\}. \tag{12}$$

Remark 3 Note that if $|\bar{w}_{J,J+1} - \bar{w}_{J-1}|\Delta x_J^{\mathrm{new}} = |\bar{w}_{J+2} - \bar{w}_{J,J+1}|\Delta x_{J+1}^{\mathrm{new}}$, then applying (11) results in $\bar{w}_J^{\mathrm{new}} = \bar{w}_{J-1}$ and $w_{J+1}^{\mathrm{new}} = \bar{w}_{J+2}$, which will be important in proving Proposition 2.1.

6. The mesh, generated in step **4**, may become irregular if the points $x_{J+\frac{1}{2}}^{\mathrm{new}}$ and $x_{J+\frac{3}{2}}$ get too close (for simplicity, we assume that except for the two cells adjusted to the fluid interface, the mesh is uniform and $\Delta x_j \equiv h$ for $j \neq J$ or $J+1$). In

order to avoid such a situation, we may need to make another local mesh adjustment followed by another conservative projection. To this end, we proceed as follows.

If $\Delta x_{J+1}^{\text{new}} > \frac{h}{2}$, no mesh rearrangement is needed and we set

$$\bar{\mathbf{w}}_J(t+\Delta t) = \bar{\mathbf{w}}_J^{\text{new}}, \quad \bar{\mathbf{w}}_{J+1}(t+\Delta t) = \bar{\mathbf{w}}_{J+1}^{\text{new}}.$$

Otherwise, the $(J+1)$-st cell is considered to bee too small and is united with the $(J+2)$-nd cell, while the "large" J-th cell is split into two cells — $(x_{J-\frac{1}{2}}, x_{J-\frac{1}{2}}+h)$ and $(x_{J-\frac{1}{2}}+h, \hat{x}_{\text{int}}^{\text{new}})$: this way we obtain the new J-th, $(J+1)$-st, and $(J+2)$-nd cells. At this point, the size of the cells is h except for the $(J+1)$-st and $(J+2)$-nd cells. In order to locally project the cell averages $\bar{\mathbf{w}}_J^{\text{new}}$, $\bar{\mathbf{w}}_{J+1}^{\text{new}}$, and $\bar{\mathbf{w}}_{J+2}$ onto the new mesh, we first use a nonlinear limiter to construct a conservative (essentially) non-oscillatory polynomial interpolant over the interval $(x_{J-\frac{1}{2}}, \hat{x}_{\text{int}}^{\text{new}})$, for example, a linear interpolant

$$\bar{\mathbf{w}}_J^{\text{new}} + \mathbf{s}_J \left(x - \frac{x_{J-\frac{1}{2}} + \hat{x}_{\text{int}}^{\text{new}}}{2} \right),$$

where the slopes $\mathbf{s}_J$ are computed component-wise. Then, the data is locally re-averaged, and the new cell averages are:

$$\bar{\mathbf{w}}_J = \bar{\mathbf{w}}_J^{\text{new}} + \left(\frac{h}{2} - \frac{\hat{x}_{\text{int}}^{\text{new}} - x_{J-\frac{1}{2}}}{2} \right) \mathbf{s}_J, \quad \bar{\mathbf{w}}_{J+1} = \bar{\mathbf{w}}_J^{\text{new}} + \frac{h}{2}\mathbf{s}_J,$$

$$\bar{\mathbf{w}}_{J+2}(t+\Delta t) = \frac{(x_{J+\frac{3}{2}} - \hat{x}_{\text{int}}^{\text{new}})\bar{\mathbf{w}}_{J+1}^{\text{new}} + h\bar{\mathbf{w}}_{J+2}}{x_{J+\frac{5}{2}} - \hat{x}_{\text{int}}^{\text{new}}}.$$

Remark 4 The evolution in step **1** can be carried out by any conservative FV scheme, whose numerical flux satisfies the essentially three-point consistency:

$$\mathbf{H}_{j+\frac{1}{2}}(\cdot, \mathbf{w}, \mathbf{w}, \cdot) \equiv \mathbf{f}(\mathbf{w}) \quad \forall j. \tag{13}$$

PROPOSITION 2.1 The above algorithm is exact for single moving contact waves provided the conservative quantities $\bar{\mathbf{w}}$ are evolved by a one-step explicit conservative FV scheme with a numerical flux satisfying (13).

Proof Suppose that at some time t, $\bar{\rho}_j = \rho_l$ for $j < J+\frac{1}{2}$, $\bar{\rho}_j = \rho_r$ for $j > J+\frac{1}{2}$, and $p_j \equiv p$ and $u_j \equiv u$ are constants for all j. It is clear that due to the flux property (13) and the CFL restriction on the time step, $\bar{\mathbf{w}}_j(t+\Delta t) = \bar{\mathbf{w}}_j$ for $j \neq J, J+1$. Computing $\bar{\mathbf{w}}_J(t+\Delta t)$ and $\bar{\mathbf{w}}_{J+\frac{1}{2}}(t+\Delta t)$ and using (10), we obtain the following "double-cell" averages:

$$\begin{aligned}
\bar{\mathbf{w}}_{J,J+1}(t+\Delta t) &= \bar{\mathbf{w}}_{J,J+1}(t) - \frac{\Delta t}{\Delta x_J + \Delta x_{J+1}} \Big[\mathbf{H}_{J+\frac{3}{2}} - \mathbf{H}_{J-\frac{1}{2}} \Big] \\
&= \bar{\mathbf{w}}_{J,J+1}(t) - \frac{\Delta t}{\Delta x_J + \Delta x_{J+1}} \Big[\mathbf{f}(\mathbf{w}_r) - \mathbf{f}(\mathbf{w}_l) \Big] \\
&= \frac{(\Delta x_J + u\Delta t)\mathbf{w}_l + (\Delta x_{J+1} - u\Delta t)\mathbf{w}_r}{\Delta x_J + \Delta x_{J+1}},
\end{aligned}$$

where $\mathbf{w}_k := \left(\rho_k, (\rho u)_k = \rho_k u, E_k = \frac{p}{\gamma_k - 1} + \frac{1}{2}\rho_k u^2\right)^T,\ k \in \{l, r\}$.

To complete the proof, it suffices now to verify that after carrying steps **3**–**5** of the algorithm out, $\bar{\mathbf{w}}_J^{\text{new}}$ will be equal to $\mathbf{w}_l$ and $\bar{\mathbf{w}}_{J+1}^{\text{new}}$ will be equal to $\mathbf{w}_r$. Indeed, since the velocity is constant, $\Delta x_J^{\text{new}} = \Delta x_J + u\Delta t$ and $\Delta x_{J+1}^{\text{new}} = \Delta x_{J+1} - u\Delta t$, and therefore *Remark* 3 applies to the case under consideration. Finally, note that even when the cells must be rearranged according to step **6** of the algorithm, the projection there will be reduced to the re-averaging of the same constant functions, and thus the proof is complete.

3 Numerical Examples

In this section, we illustrate the performance of the new locally moving mesh finite-volume-particle (LMM-FVP) method. We also compare the obtained results with the corresponding solutions computed by the finite-volume-particle (FVP) method but without applying the locally moving mesh algorithm in §2.1, and with the corresponding results of the single fluid computations. In our examples, we use the generalized minmod piecewise linear reconstruction [SWE 84, NES 90, LIE 03] and the Euler method for the time evolution, so that the resulting central-upwind scheme is (formally) second-order in space and first-order in time.

Example 1 — Single Contact Wave. We first consider the system (1)–(2),(4) subject to the following Riemann initial data:

$$(\rho, u, p, \gamma)^T = \begin{cases} (1.0, 1.0, 1.0, 1.6)^T, & \text{if } x < 0.25, \\ (0.1, 1.0, 1.0, 1.4)^T, & \text{if } x > 0.25. \end{cases}$$

We apply the MML-FVP method with 100 cells for the central-upwind scheme and 100 particles that are initially placed in the cell centers. The minmod parameter is $\theta = 2$, and the final time is $t = 0.5$. The solutions computed by the LMM-FVP and FVP methods are plotted in Figure 1. As predicted by Proposition 2.1, all the oscillation generated by the FVP method, have been completely eliminated using our locally moving mesh algorithm.

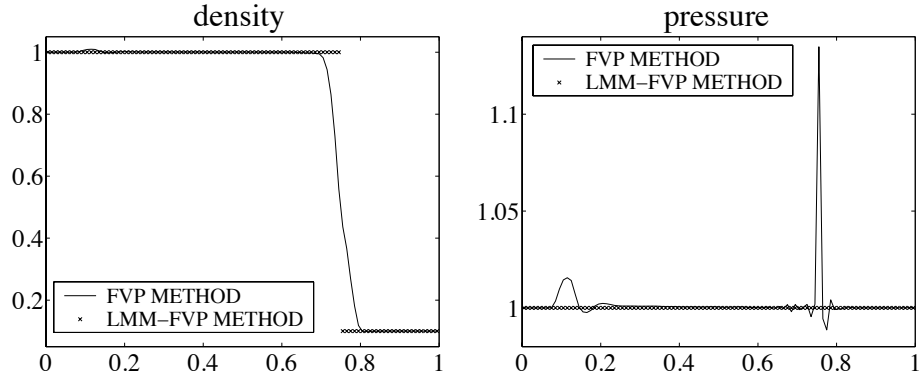

Figure 1: Single contact wave (ρ and p) by the LMM-FVP and FVP methods.

Example 2 — Shock-Tube Problem. In this example, the system (1)–(2),(4) is considered subject to the two different Riemann data:

$$(\rho, u, p, \gamma)^T = \begin{cases} (1.000, 0.1, 1.0, \gamma_l)^T, & \text{if } x < 0.5, \\ (0.125, 0.0, 0.1, \gamma_r)^T, & \text{if } x > 0.5. \end{cases} \tag{14}$$

The first set of initial data are for the two-fluid problem with $\gamma_l = 1.4$ and $\gamma_r = 1.2$. In Figure 2, we plot the solution at time $t = 0.25$ computed by the LMM-FVP method on the grids with 200 and 800 cells and the same number of particles that are uniformly distributed at $t = 0$. The minmod parameter $\theta = 1.3$. Even though there are some small pressure/velocity oscillations and also some oscillations at the rarefactions corners (both oscillations seem to decrease as the mesh is refined), one can observe a very high quality of the computed solution, especially at the contact discontinuity. For the purpose of comparison, we also consider the single fluid problem with the same initial data (14), but with $\gamma_l = \gamma_r = 1.4$. The solution computed by the FVP method at $t = 0.25$ and with the same number of cells/particles is shown in Figure 3. As one can see, the overall quality of the computed solutions is comparable, but the LMM-FVP method, applied to the two-fluid problem, provides a much better resolution of the contact wave than the FVP method, realized on the uniform mesh for the single fluid model.

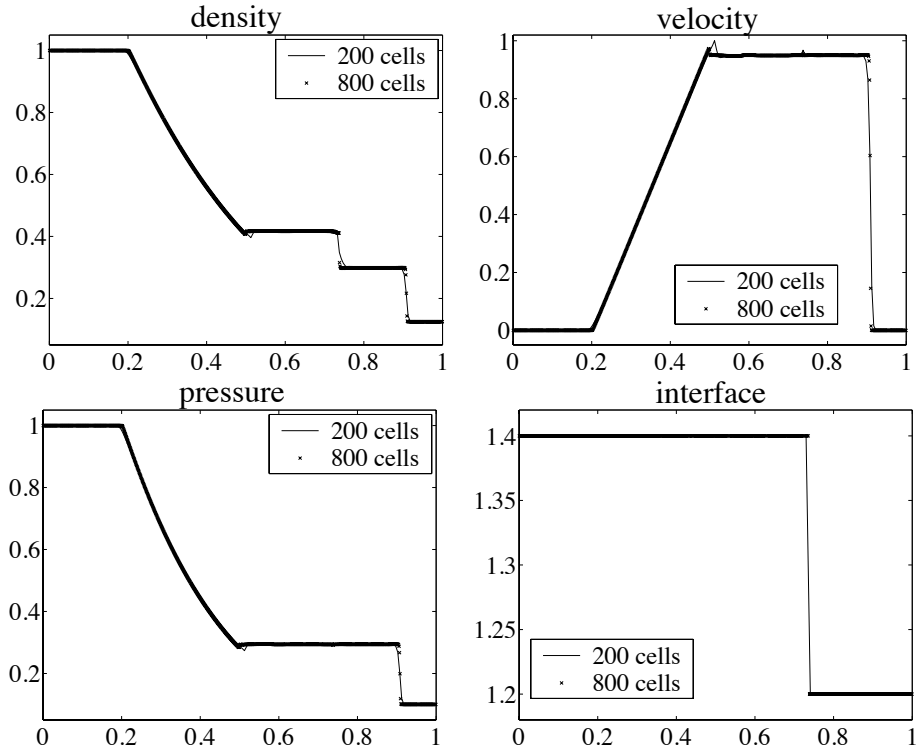

Figure 2: Two-fluid shock-tube problem by the LMM-FVP method.

Acknowledgment. The work of A. Chertock was supported in part by the NSF Grant # DMS-0410023. The research of A. Kurganov was supported in part by the NSF Grant # DMS-0310585.

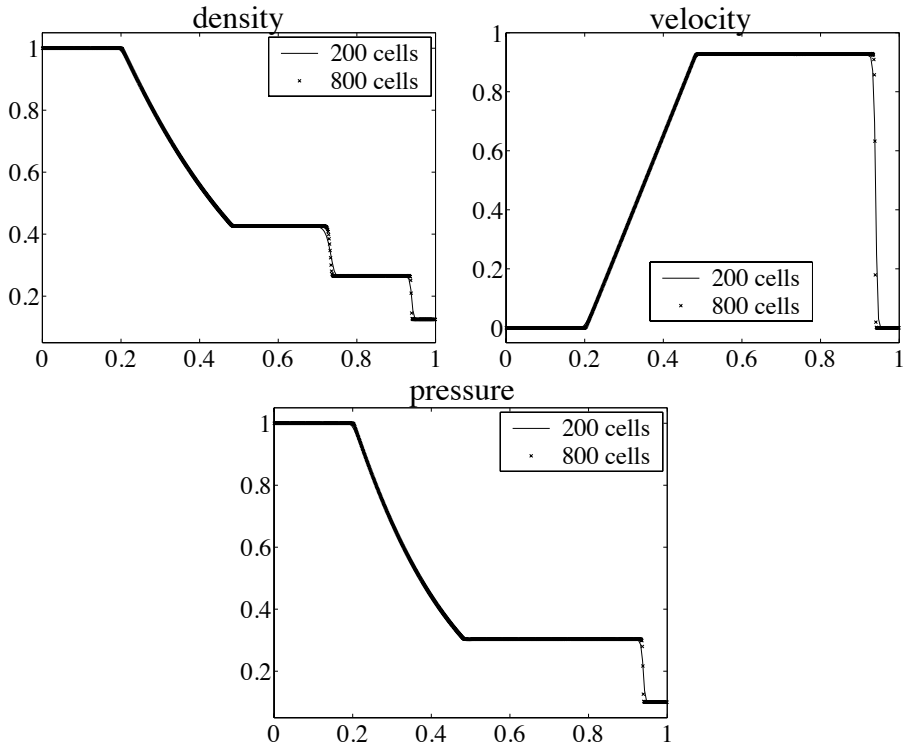

Figure 3: Single fluid shock-tube problem by the FVP method.

4 Bibliography

[ABG 96] Abgrall R., (1996), "How to prevent pressure oscillations in multicomponent flow calculations: a quasi conservative approach". J. Comput. Phys., Vol. 125, pp. 150–160.

[ABG 01a] Abgrall R., Karni S., (2001), "Ghost-fluids for the poor: a single fluid algorithm for multifluids". Hyperbolic problems: theory, numerics, applications, Vol. I, II (Magdeburg, 2000), pp. 1–10, Internat. Ser. Numer. Math., Vol. 140, Birkhäuser, Basel.

[ABG 01b] Abgrall R., Karni S., (2001), "Computations of Compressible Multifluids". J. Comput. Phys., Vol. 169, pp. 594–623.

[CHE 04] Chertock A., Kurganov A., (2004), "On a hybrid finite-volume-particle method". M2AN Math. Model. Numer. Anal., Vol. 38, pp. 1071–1091.

[CHEa] Chertock A., Kurganov A., "On practical implementation of particle methods". Submitted to Appl. Numer. Math.

[CHEb] Chertock A., Kurganov A., Petrova G., "Finite-Volume-Particle Methods for Models of Transport of Pollutant in Shallow Water". J. Sci. Comput., to appear.

[COC 97] Cocchi J.-P., Saurel R., (1997), "A Riemann problem based method for the resolution of compressible multimaterial flows". J. Comput. Phys., Vol. 137, pp. 265–298.

[FED 99] Fedkiw R. P., Aslam T., Merriman B., Osher S., (1999), "A non-oscillatory Eulerian approach to interfaces in multimaterial flows (the ghost fluid method)". J. Comput. Phys., Vol. 152, pp. 457–492.

[FIL 64] Filippov, A. F., (1964), "Differential equations with discontinuous right-hand side". A.M.S. Transl., Vol. 42, pp. 199–231.

[FIL 88] Filippov, A. F., (1988), "Differential equations with discontinuous right-hand side". Mathematics and its Applications (Soviet Series), Kluwer Academic Publishers Group (Dordrecht, Vol. 18).

[KAR 94] Karni S., (1994), "Multicomponent flow calculations by a consistent primitive algorithm". J. Comput. Phys., Vol. 112, pp. 31–43.

[KRÖ 97] Kröner D., (1997), "Numerical schemes for conservation laws". Wiley, Chichester.

[KUR] Kurganov A., Lin C.-T., "On the reduction of numerical dissipation in central-upwind schemes". In preparation.

[KUR 01] Kurganov A., Noelle S., Petrova G., (2001), "Semi-discrete central-upwind scheme for hyperbolic conservation laws and Hamilton-Jacobi equations". SIAM J. Sci. Comput., Vol. 23, pp. 707–740.

[KUR 00a] Kurganov A., Petrova G., (2000), "Central schemes and contact discontinuities". M2AN Math. Model. Numer. Anal., Vol. 34, pp. 1259–1275.

[KUR 00b] Kurganov A., Tadmor E., (2000), "New high-resolution central schemes for nonlinear conservation laws and convection-diffusion equations". J. Comput. Phys., Vol. 160, pp. 241–282.

[LEV 02] LeVeque R., (2002), "Finite volume methods for hyperbolic problems". Cambridge Texts in Applied Mathematics, Cambridge University Press, Cambridge.

[LIE 03] Lie K.-A., Noelle S., (2003), "On the artificial compression method for second-order nonoscillatory central difference schemes for systems of conservation laws". SIAM J. Sci. Comput., Vol. 24, pp. 1157–1174.

[NES 90] Nessyahu H., Tadmor E., (1990), "Non-oscillatory central differencing for hyperbolic conservation laws". J. Comput. Phys., Vol. 87, pp. 408–463.

[RAV 85] Raviart P.-A., (1985), "An analysis of particle method". In Numerical Methods in Fluid Dynamics (Como, 1983), pp. 243–324, Lecture Notes in Math., Vol. 1127, Springer-Verlag, Berlin.

[ROE 84] Roe P. L., (1984), "A new approach to computing discontinuous flows of several ideal gases". Technical Report, Granfield Institute of Technology.

[SWE 84] Sweby P. K., (1984), "High resolution schemes using flux limiters for hyperbolic conservation laws". SIAM J. Numer. Anal., Vol. 21, pp. 995–1011.

[WAC 04] Wackers J., Koren B., (2004), "Five-equation model for compressible two-fluid flow". Report MAS-E0414, CWI, Amsterdam.
`http://ftp.cwi.nl/CWIreports/MAS/MAS-E0414.pdf`